CHALMERS
UNIVERSITY OF TECHNOLOGY

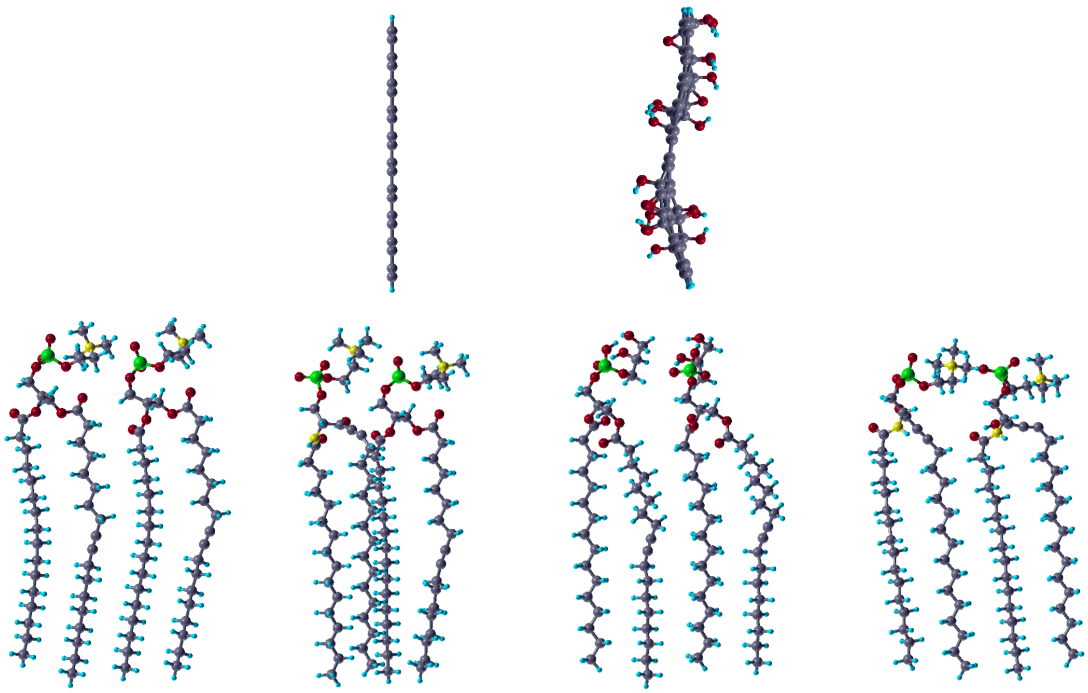

Computational modelling of phospholipids in plasma membranes

A dive into the diverse response of bacteria and mammalian cells to graphene and graphene oxide

Master's thesis in Nanotechnology

VICTOR LANAI

Department of Microtechnology and Nanoscience (MC2)
CHALMERS UNIVERSITY OF TECHNOLOGY
Gothenburg, Sweden, 2022

Master's thesis 2022

Computational modelling of phospholipids in plasma membranes

A dive into the diverse response of bacteria and mammalian cells to graphene

VICTOR LANAI

Department of Microtechnology and Nanoscience (MC2)
Division of Quantum Device Physics Laboratory
CHALMERS UNIVERSITY OF TECHNOLOGY
Gothenburg, Sweden, 2022

Computational modelling of phospholipids in plasma membranes
A dive into the diverse response of bacteria and mammalian cells to graphene

VICTOR LANAI

Supervisor and examiner
Professor Elsebeth Schröder
Department of Microtechnology and Nanoscience (MC2)
Chalmers University of Technology

Master's Thesis 2022 (MCCX04)
Chalmers University of Technology
Department of Microtechnology and Nanoscience (MC2)
Quantum Device Physics Laboratory
SE-412 96, Gothenburg, Sweden
+46 (0)31-772 10 00
www.chalmers.se

Cover: Phospholipid pairs together with a graphene- and graphene oxide flake.

Typeset in LaTeX
Figures created using XCrysDen

Gothenburg, Sweden, 2022

Computational modelling of phospholipids in plasma membranes
A dive into the diverse response of bacteria and mammalian cells to graphene
VICTOR LANAI
Department of Microtechnology and Nanoscience (MC2)
Chalmers University of Technology

Abstract

The purpose of this project was to investigate if the constituents of phospholipids in plasma membranes affect how cells interact with graphene (G) and graphene oxide (GO). It has previously been shown that vertically grown graphene flakes are effective in killing bacteria whilst keeping mammalian cells intact. However, the mechanism behind this phenomena is not known, and is at the same time difficult to measure experimentally. Therefore we choose density functional theory as a tool, with the goal to enhance the understanding. This thesis dives into the plasma membranes of bacterial and mammalian cells, and target different phospholipids in these membranes. The project started off by creation of a library of single phospholipids. These were put together into systems of pairs for calculation of bonding between different phospholipids. Further, both a G and a GO flake were created, and incorporated into the systems with the phospholipid pairs. Analysis of the interaction energies between these flakes with the phospholipid pairs was performed, both when the flakes approach the phospholipids, and upon penetration of the membrane. Calculations show that the most abundant phospholipids in mammalian cells have stronger bonding to each other, compared to bacterial phospholipids. Further, when the G/GO flakes enter between the phospholipid pairs, the bacterial pair exhibits less repulsive interactions, and a more stable system with the flakes were found. Therefore, these variables may contribute to the diverse robustness between bacterial and mammalian cells, and thus, the composition of phospholipids can be an important factor in explaining the difference in viability between organisms.

Keywords: Density Functional Theory, Microorganism, Bacteria, Eukaryotes, Mammalian, Graphene, Graphene oxide

Acknowledgements

First of all, I would like to thank my supervisor Elsebeth Schröder for your fantastic guidance in density functional theory, your enthusiasm for the project and all valuable support during these months. You opened my eyes to molecular modeling and made me appreciate the world of quantum physics. This work was also done in collaboration with Ivan Mijakovic and Shadi Rahimi at the division of Systems and Synthetic Biology. I greatly appreciate your interest and suggestions for molecules to target. I am also thankful to everyone at the Quantum Device Physics Laboratory for creating a wonderful work atmosphere.

This has been an amazing experience and I'm very grateful for the opportunity to do this project. I am really looking forward to continuing these collaborations, and believe that together, we push the boundaries.

Victor Lanai
Gothenburg, Sweden, June 2022

Contents

Acronyms

Below is the list of acronyms that have been used throughout this thesis listed in alphabetical order:

a.u	Atomic units
C	Carbon
Ca	Calcium
CD	Communicable diseases
CL	Cardiolipin
CVD	Chemical vapor deposition
DFT	Density functional theory
DNA	Deoxyribonucleic acid
G	Graphene
GGA	Generalized gradient approximation
GO	Graphene oxide
H	Hydrogen
HF	Hartree-Fock
HK	Hohenberg-Kohn
KS	Kohn-Sham
LDA	Local density approximation
LSDA	Local spin density approximation
N	Nitrogen
Na	Sodium
O	Oxygen
OH	Hydroxide
P	Phosphorous
PBE	Perdew-Burke-Ernzerhof functional
PC	Phosphatidylcholine
PG	Phosphatidylglycerol
PP	Pseudopotential
PW91	Perdew-Wang functional
SCF	Self-consistence field
SE	Schrödinger equation
SM	Sphingomyelin
TF	Thomas-Fermi
vdW	Van-der-Waals
vdW-DF	Van-der-Waals density functional
WHO	The World Health Organisation

Nomenclature and constants

$\hat{H}$	Hamiltonian operator
Ψ	Wave-function
i	Imaginary unit $[i^2 = -1]$
$\hbar$	Reduced Planck constant $[6.582119569 \times 10^{-16}$eV s]
∂	Derivative
t	Time
E	Energy (eigenvalue)
m	Mass
∇	Laplace operator (three-dimensional derivative)
V	Potential energy [electron-nuclei]
U	Potential energy [electron-electron] or [nuclei-nuclei]
N	Number of particles
χ_1	Orbital function
$\vec{x_1}$	Spin [up or down]
$\hat{J}$	Coulomb operator
$\hat{K}$	Exchange operator
$n(\vec{r})$	Electron density
T	Kinetic energy
G	Universal functional
μ	Lagrange parameter
ϕ	Kernel function

Conversions

Ry	13.6056980659 eV
eV	1.60218×10^{-19} J
mol	$6.02214076 \times 10^{23}$ units

Elements

Below is a description of the representative colour of each atom that have been used in figures throughout this thesis:

●	Hydrogen
●	Carbon
●	Oxygen
●	Nitrogen
●	Phosphorous

1
Introduction

Today, computational modelling and simulations are a mainstream tools in many sectors for a variety of causes. From the simulations, certain outcomes are predicted, which for example enhances safety, speeds up product development or increases profitability. A house, a car or a mobile phone would not be build today without doing computational simulations [1]. For many years, the field of biology has fallen behind in the utilization of these tools, and the bottleneck in product development has become the time of trial and error [2]. Therefore, biomolecular simulations are getting more attention as a tool to streamline the time from idea to product[3]. A wide variety of softwares exist today with different depth of the target building blocks, almost like an interior designer and landscape architect differ in their work. Therefore, different approaches in computational biology could also complement each other for the best outcome [4]. In this project, the depth of quantum chemistry is implemented where the electron density of elements are considered as the outcome of simulations. This project dives into the constituents of plasma membranes of microorganisms and investigates if the varying robustness between specific cells can be explained through quantum chemistry. Phospholipids from the outer leaflet of bacteria and mammalian cell are simulated as isolated molecules and in pairs, in combinations relevant for the membranes. The interaction with graphene and graphene oxide, as intersected into the membrane is also considered.

Microorganisms can be found almost everywhere and are good illustrations of cellular life on earth. Bacteria and eukaryotes are two kinds that have been evolved for a long time to extremely diverse organisms with numerous of different forms and shapes [5]. Bacteria has a key role in the maintenance of the environment and only a small fraction is causing infections and diseases [6]. These bacteria are pathogens for some communicable diseases (CD) [7]. CDs are diseases that can be spread from one person to another via a variety of ways and are considered to have a major negative effect on the well being worldwide. Development of compounds for killing bacteria has increased over the years and has in many cases been successful, by reducing diseases. There are, however, many infectious bacteria still evolving and challenges to treat these are arising. The World Health Organization (WHO) has declared that antimicrobial resistance is one of the top ten threats to human health [8], which has, for example, made healthcare-related infections a major issue worldwide [9].

The emergence of new material and technologies helps to accelerate development and possible solutions. Graphene is a material that has received a lot of attention lately, due to its wide range of uses. This has lead to different projects around the world, among these is The Graphene Flagship, funded by the European Union and coordinated by Chalmers University of Technology. This foundation includes many different work packages, with the goal to take graphene from small scale laboratory work, into large scale manufacturing. Many sectors are suggested to take advantage of graphene, with the health sector as a potential candidate [10]. In an article from 2018, researchers showed that vertically grown graphene flakes are effective in killing bacteria, whilst keeping mammalian (eukaryotic) cells intact [11]. Therefore, graphene has the possibility of targeting pathogenic bacteria. However, regulation of this treatment is still a challenge and the mechanism behind this phenomena is fully not known, and is at the same time difficult to measure experimentally. Therefore we choose density functional theory (DFT) as a tool with the goal to enhance the understanding. DFT is a computational method which calculates the electron density at the quantum level.

The project started off by creation of a library of single phospholipids. These were further simulated together in pairs, with the purpose to analyze interactions between different phospholipids. A graphene- and graphene oxide ”flake” were also created in an isolated form, and then incorporated into the systems with the phospholipid pairs. Simulations of these flakes approaching the heads of each pair were performed together with analysis of penetration depth and separation distance between each pairs.

2

Theory and materials

This chapter introduces some of the theory behind the chosen methods, and background to the relevancy of performing simulations of phospholipids and graphene and graphene oxide. It begins with a general description of cellular structures and narrows in on phospholipids of plasma membranes and how their constituents differ between organisms. This is followed up with a small passage of the characteristics of graphene and some methods for fabrication. The chapter ends with a section dedicated to DFT and some historical steps towards the algorithm of today.

2.1 Cellular diversity between bacteria and mammalian (eukaryotic)

In order not to get confused about words like eukaryotic, bacteria and mammalians, a quick explanation is in place. Mammalians are part of the animal world, where humans are included. Mammalians cells are multicellular and considered within the eukaryotes. Therefore, to simplify it, when referring to eukaryotes in the following sections we also mean mammalian [12].

For development of different drugs or materials for the purpose to treat certain diseases, it is important to distinguish between the pathogenic source and the healthy ones. This increases the likelihood that the substance will fulfill its purpose with minimized side-effects. Therefore, understanding cellular structures is important for targeting specific sites within certain organisms. This project will not explain every single detail of each organism, but it will show some general theory of the building blocks within an organism, and how these differ between bacteria and mammalian cells.

The most fundamental observed dissimilarity between bacteria and eukaryotic is the size and morphological complexity (with some exceptions, which is ignored in this description). All bacteria are so-called prokaryotes and unicellular, while the eukaryotes are multicellular organisms, where the cells have different functions. Bacteria has been present since approximately 1100 million years after the creation of the earth and eukaryotes were not present until at least 1500 millions years after the bacterial introduction. According to the endosymbiotic theory, the coexistence of prokaryotic cells gave rise to the eukaryotes [13], which lead to a larger and more complex cell structure for the eukaryotes. Other than size, are the presence of membrane-bound organelles within eukaryotic cells is a major factor to the diverse complexity, which bacteria lacks [14].

The aim of this project is to investigate interactions between graphene and the plasma membrane of mammalian and bacterial cells. Therefore, description of lipids, and certainly phospholipids, is of high relevance, since they are the main constituent of plasma membranes. Lipids can be classified into different categories, but the main characteristic of all lipids is that they have little or no solubility in water. Some lipids can be synthesized inside the cell and some are essential nutrition for proper function. The type of synthesized lipid also differs between different organisms and therefore, the constituent of plasma membranes can look a bit different between bacteria and eukaryotes. Lipids can be divided into different classes based on the structural chemistry and additional characteristic similarities. The key component of cell membranes is the class of phospholipids. They are amphiphilic, with a hydrophobic ”tail” and a hydrophilic ”head” (fig.2.1). The tail is usually derived from fatty acids, a carboxylic acid attached to an aliphatic chain. The length and degree of saturation of the aliphatic chain can differ between different fatty acids. The head is polar and comprises of a phosphate group esterified to an alcohol group of varying length and chemical structure. Since phospholipids consist of both a water- and a fat loving moiety, they have the capacity to stack into phospholipid layers, the heads pointing towards water and the tails attracting each other [15]. Phospholipids can stack into bilayers and aggregate into longer sheets, which forms the majority of plasma membranes [16]. The constituent of these phospholipids could vary between different cell types, and therefore, might be a factor to the survival response to graphene ”spikes”.

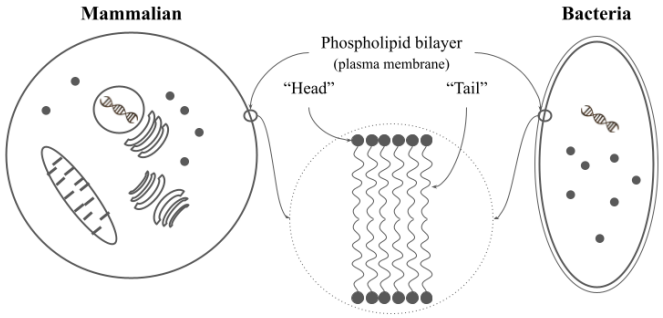

Figure 2.1: Generalized structure of mammalian- and bacterial cells with magnified view of stacking phospholipids in the plasma membranes

To attempt an understanding of the chemistry of life and for the possibility to simulate these systems, it is also necessary to dive deeper into the basic elements of living organisms, also called the biogenic elements. Carbon (C), hydrogen (H), oxygen (O) and nitrogen (N) are the most abundant and account for around 96% of all microorganisms. These together with phosphorous (P) and calcium (Ca) are the primary elements of biological systems. Secondary elements usually exist as salts or ions and are found in much lower quantities. The third category is the trace elements which are present in very low amounts. Some of these elements form covalent bonds with each other into biological molecules, while some elements exist as co-factors and are essential for proper enzymatic activity. As stated above, the purpose of this project is to target different phospholipids of plasma membranes in mammalian and bacterial cells. Phosphatidylcholine (PC) and sphingomyelin (SM) are two of the most abundant phospholipids in the outer leaflet of mammalian plasma membranes [17][18], while cardiolipin (CL) and phosphatidylglycerol (PG) were found to be two of the most abundant in bacterial plasma membranes [19]. These phospholipids constitute of the primary elements (C, H, O, N, P) and therefore, these five elements are the building blocks in this thesis.

2.2 Graphene and graphene oxide

Graphene, a single layer of C atoms, derived from graphite. The C atoms within graphene form a two-dimensional flat monolayer and are bonding to each other in a honeycomb lattice. Graphene has been studied for decades, and it was assumed to be unstable and not exist in the free state. This was proven wrong in 2004 when the isolation of graphene was discovered together with the experimental fact that it exhibits great crystalline quality and macroscopic continuity [20][21]. When graphene layers are stacked on top of each other, as in graphite, they bind through van der Waals forces. The shift from two dimensional material to three dimensional usually is taken to be at approximately 10 layers of graphene [22]. The ground state of a neutral single C atom is occupied by six electrons where four are in the outer shell, also called the valence electrons. The nature of the orbital for a free C atom is therefore described as $1s^2 2s^2 p^2$ with two of the valence electrons occupying in the $2s$ orbital and two in the $2p$. In graphene, one C atom is bounded to two neighbours through orbital hybridisation. Thus, three of the four valence electrons form σ-bonds to their neighbour, and the remaining electron is occupying the p orbital perpendicular to the graphene plane. The honeycomb structure together with orbital hybridisation is one of the main reasons for the excellent properties of graphene [23].

Since the isolation of graphene as a stable 2D material, many groups have been working on methods for suitable fabrication. This is a challenging task and utilization of graphene is highly dependent on the fabrication method. One way is exfoliation, which is a top-down approach where van der Waals forces within graphite are overcome to obtain individual graphene layers. This can be done mechanically or chemically. Mechanical exfoliation peels off graphene layers mechanically and is done by shearing or milling. Shearing mechanically was the first method for the isolation of graphene and in that study, scotch-tape was used, now referred to as the scotch-tape technique. This is a simple method and provides graphene layers with high crystalline and electronic quality, but it is also time-consuming and thus, not suitable for large-scale production. Chemical, also called liquid-phase exfoliation produces graphene with a much higher throughput, making it suitable for rapid industrial scale. This technique starts by breaking down graphite into smaller flakes, then, by introducing solvents and ultrasound, the graphite flakes are further split into individual graphene layers. This is also a simple method with the advantage of low cost, but the downside is a product with possibility of uncontrolled defects and thus, lower quality. A bottom-up technique is chemical vapor deposition (CVD), which creates an epitaxial layer by the growth of a crystalline material onto another crystalline substrate. This has been used for vertically grown graphene flakes and was done for the study of the bactericidal effects of graphene. To get purified graphene layers, it is necessary to edge away the crystalline substrate. This can be done by chemicals and the obtained graphene is usually of high quality [24][25][26].

2.3 The route to density functional theory

The computational method used in this thesis is density functional theory (DFT), for which a short overview is given here. Density functional theory (DFT) is equivalent to the fundamental equation of quantum mechanical systems, the Schrödinger equation (SE)[27][28]. In 1926, Erwin Schrödinger published a series of papers where he postulated "that material points consist of, or are nothing but, wave-systems" and derived this into the mathematical equation

$$\hat{H}\Psi = i\hbar\frac{\delta}{\delta t}\Psi \tag{2.1}$$

which is also called the time-dependent SE [29]. A simplified form for time invariant potentials, is the time-independent, non-relativistic SE

$$\hat{H}\Psi = E\Psi \tag{2.2}$$

where $\hat{H}$ is the Hamilton operator for the system and Ψ is the wave function to a set of eigenstates of the Hamiltonian with the associated eigenvalue E. With variational methods, the solution for the lowest eigenvalue of a stationary state can in principle be found, hence the ground state. Schrödinger set by these expressions the foundation for the future theory of quantum mechanical systems. Both the time-dependent and the time-independent SE are what many scientist in the quantum field have been trying to solve over the years, but exact solutions are not possible for more than a few particles. Therefore, many approaches to these equations have been evolved and one of these is the DFT, which is exact as the time-independent SE, but to solve it for practical purposes, approximations are used. In eq.(2.2), the Hamiltonian is used and the time-independent SE can be expressed as

$$\Big[-\frac{\hbar}{2m_i}\sum_{i=1}^{N}\nabla_i^2 - \frac{\hbar}{2m_a}\sum_{a=1}^{M}\nabla_a^2 + \sum_{i=1}^{N}\sum_{a=1}^{N}V(r_i,r_a) + \sum_{i=1}^{N}\sum_{j>1}^{N}U(r_i,r_j) + \sum_{a=1}^{N}\sum_{b>1}^{N}U(r_a,r_b)\Big]\Psi = E\Psi \tag{2.3}$$

with the two first expressions being the kinetic energy for the electrons (i) and nuclei (a). The three last terms are the potential energy of the system and represent the attractive electrostatic interaction between electron(i)-nuclei(a) and the repulsive potential between electron(i)-electron(j) and nuclei(a)-nuclei(b). SE has been solved exactly for a single-particle system where models like particle in a box and harmonic oscillator have been used to describe these problems. For a many-body system where multiple particles are interacting the SE becomes more complicated which makes exact analytical calculations impossible. Several models have been developed during the years to deal with this problem, and until now, all models rely on approximations of various kinds.

One improvement is to realize that the atoms and electrons move on very different timescales, due to the mass differences (the mass of the electron is at least a factor 2000 smaller than the atom). In 1927, this was recognized by Max Born and J. Robert Oppenheimer [30], who proposed the Born-Oppenheimer approximation. The consequence is that the system can be approximated by considering the electron moving in the field of fixed nuclei. This means, roughly speaking, that the kinetic energy from the nuclei is zero and the nuclei-nuclei repulsion is a constant. The Hamiltonian can therefore be split and reduced to

$$\hat{H} = -\frac{\hbar}{2m_i}\sum_{i=1}^{N}\nabla_i^2 + \sum_{i=1}^{N}V(r_i) + \sum_{i=1}^{N}\sum_{j>1}^{N}U(r_i,r_j) \tag{2.4}$$

Further approximation to the many-body system was done by Douglas Rayner Hartree and Vladimir Aleksandrovich Fock [31][32] by simplifying the wave function into a Slater determinant [33]

$$\Psi_{SD} = \frac{1}{\sqrt{N!}}det\begin{bmatrix} \chi_1(\vec{x_1}) & \chi_2(\vec{x_1}) & ... & \chi_N(\vec{x_1}) \\ \chi_1(\vec{x_2}) & \chi_2(\vec{x_2}) & ... & \chi_N(\vec{x_2}) \\ . & . & . & . \\ . & . & . & . \\ . & . & . & . \\ \chi_1(\vec{x_N}) & \chi_2(\vec{x_N}) & ... & \chi_N(\vec{x_N}) \end{bmatrix} \tag{2.5}$$

where $\chi_1(\vec{x_1})$ denotes the spin orbitals and are composed of two spin functions, up or down, and a spatial orbital. They expressed the so called Hartree-Fock (HF) approximation as

$$\hat{H}_{HF}\Psi_{SD} = E_{HF}\Psi_{SD} \tag{2.6}$$

The Hamiltonian in the HF approximation still contains the contribution from the kinetic energy, the electron-nuclei attraction and the electron-electron repulsion. The electrostatic electron-electron interaction was expressed as an average repulsive potential each electron experiences from its surrounding electrons, also called

the HF potential (V_{HF}), and expressed as

$$V_{HF} = \sum_{j}^{N} (\hat{J}_j(\vec{x_1}) - \hat{K}_j(\vec{x_1})) \tag{2.7}$$

The HF potential includes $\hat{J}_j$ and represents the Coulomb operator, the electron-electron repulsion from the j-th orbital. The $\hat{K}_j$ is the exchange operator and describes the electron exchange energy due to the antisymmetry of the N-electron wave function. They also took advantage of the variational principle to find the optimal wave function (Ψ_0). This principle states that if any trial wave function (Ψ_{tri}) is chosen and computed together with the Hamilton operator of the SE, the expectation value of that eigenvalue (E_{trial}) must be equal to, or higher than the true energy. Therefore, E_{trial} is used as an upper bound to the ground state energy levels and written with Dirac notations as

$$\langle \Psi_{trial} | \hat{H} | \Psi_{trial} \rangle = E_{trial} \geq E_0 = \langle \Psi_0 | \hat{H} | \Psi_0 \rangle \tag{2.8}$$

This was the birth of the self-consistent field, which is an iterative method that computes the wave-function until it converges with the true SE. Unfortunately, the HF approach is only feasible for small systems and becomes computational expensive with increased numbers of particles [27].

During the same time period, 1927, another approximation method was published, the Thomas-Fermi model [34]. Llewellyn Thomas and Enrico Fermi describe the system as a uniform electron gas where they use a statistical model to predict the behavior of a many-body system by calculating the electronic density rather than the wave function. The importance of this equation is however not in the yield of quantitative predictions, but it should be highlighted that this was the first model where the energy is expressed only in terms of the electron density. Because of its inaccuracy, the TF model did not receive too much of attention and it was not until 1964 when Pierre Hohenberg and Walter Kohn developed this further with their two Hohenberg-Kohn (HK) theorems [35], and then one year later expanded by Walter Kohn and Lu Jeu Sham into the Kohn-Sham (KS) theorem [36]. These theorems were the birth of DFT and Walter Kohn was awarded the Nobel Prize in chemistry 1998 for his contributions to computational chemistry [37].

The first HK theorem proved that the ground state energy from SE is a unique functional of the electron density $n(\vec{r})$

$$n(\vec{r}) = 2 \sum_{i} \psi_i^*(\vec{r}) \psi_i(\vec{r}) \tag{2.9}$$

They first denoted the electron density in the ground state as a functional of the external potential $V(\vec{r})$, and then by reductio ad absurdum, they proved that $n(\vec{r})$ is a unique functional of $\vec{r}$. Since the energy is dependent on $\vec{r}$, they stated that the ground state for a full many-particle system should also be a unique function of $\vec{r}$. They defined the energy functional as

$$E[n(\vec{r})] = \int V(\vec{r}) n(\vec{r}) d^3r + F[n(\vec{r})] \tag{2.10}$$

with

$$F[n(\vec{r})] = \langle \psi | T + U | \psi \rangle \tag{2.11}$$

where T is the kinetic energy and U the Coulomb electron-electron interactions. This functional was further transformed into the form

$$F[n(\vec{r})] = \frac{1}{2} \int \frac{n(\vec{r}) n(\vec{r'})}{|r - r'|} d^3r d^3r' + G[n(\vec{r})] \tag{2.12}$$

with $G[n(\vec{r})]$ as a universal functional of the density.

The second HK theorem defined an important property for the functional. The input for the true ground state density should deliver the lowest energy and thus the ground state of the system. They took advantage of the variational principle and expressed that any trial electron density $n(\vec{r})_{trial}$ is the upper bound for the true ground state as

$$\langle \Psi_{trial} | \hat{H} | \Psi_{trial} \rangle = \int V(\vec{r}) n(\vec{r})_{trial} d^3r + F[n(\vec{r})_{trial}] = E[n(\vec{r})_{trial}] \geq E_0[n(\vec{r})_0] = \langle \Psi_0 | \hat{H} | \Psi_0 \rangle \tag{2.13}$$

If the true functional were known, then the electron density could be varied until the energy from the functional is minimized and thus solve the relevant electron density. For this to be true it is necessary that minimized energy does not change the number of electrons. They used the Lagrange multiplier and expressed the condition as

$$\delta E[n(\vec{r})] - \mu \int n(\vec{r}) d^3r = 0 \tag{2.14}$$

with μ as a Lagrange parameter. This was then rearranged into

$$\delta \frac{F[n(\vec{r})]}{\delta n} + V(\vec{r}) = \mu \tag{2.15}$$

Until this point, the computational effort was reduced from 3N variables of the wave function into three spatial variables for the electron density, but they did not say what the functional actually was and solving the SE was thus still an issue. Kohn and Sham suggested how this could be approached and developed the KS equations. They introduced the concept of a single-electron wave functions. They started by assuming that there was no contribution from the electron-electron interactions and reduced the universal functional to

$$F[n(\vec{r})] = T[n(\vec{r})] \tag{2.16}$$

which is only dependent of the kinetic energy. In this way, the contribution from the kinetic energy was solved with a much higher accuracy than the former Thomas-Fermi equations. The kinetic energy was formulated as

$$T[n(\vec{r})] = \sum \int d^3r \psi_i^*(\vec{r}) \left(-\frac{\hbar}{2m_i} \sum_{i=1}^{N} \nabla_i^2 \right) \psi_i(\vec{r}) \tag{2.17}$$

Since this is the kinetic energy from a non-interacting system, they could not say that this is equal to the true kinetic energy for a interacting system. Kohn and Sham added some terms for an interacting system and expressed it as

$$F[n(\vec{r})] = T[n(\vec{r})] + U[n(\vec{r})] + E_{xc}[n(\vec{r})] \tag{2.18}$$

with $U[n(r)]$ as the Coulombic electron-electron interaction

$$U[n(\vec{r})] = \frac{1}{2} \int \int d^3r d^3r' \frac{n(\vec{r})n(\vec{r'})}{r - r'} \tag{2.19}$$

and $E_{xc}[n(r)]$ as the exchange-correlation energy. This expression is solved approximately and contains everything unknown from the kinetic energy of a interacting system together with the potential energy from self-interacting effects. The equation to be minimized is now

$$E[n(\vec{r})] = T[n(\vec{r})] + V[n(\vec{r})] + U[n(\vec{r})] + E_{xc}[n(\vec{r})] \tag{2.20}$$

and from the constraints of the Lagrange multiplier

$$\delta E[n(\vec{r})] - \sum \epsilon_i \int d^3r \psi^*(\vec{r}) n(\vec{r}) \psi(\vec{r}) = 0 \tag{2.21}$$

with ϵ_i as the i-th Lagrange parameter, the KS equations were reduced to a one-particle SE and took the form

$$\left[-\frac{\hbar^2}{2m} \nabla^2 + V_{KS}(\vec{r}) \right] \psi_i(\vec{r}) = \epsilon_i \psi_i(\vec{r}) \tag{2.22}$$

with the KS potential as

$$V_{KS}(\vec{r}) = V(\vec{r}) + U(\vec{r}) + E(\vec{r}) = \int V(\vec{r}) n(\vec{r}) d^3r + e^2 \int \frac{n(\vec{r'})}{|r - r'|} d^3r' + \frac{\delta E_{xc}[n(\vec{r})]}{\delta n(\vec{r})} \tag{2.23}$$

To solve the KS equations it is necessary to know the single-electron wave function to get the electron density. But to find the single-electron wave function the KS equations need to be solved. To break this circle, Kohn and Sham took advantages of the self-consistent field from HF equations and the problem was treated by an iterative method. This is done by first defining a trial electron density $n(\vec{r})_{trial}$ and use this to solve the KS equations, which will yield the single-electron wave functions $\phi_i(\vec{r})$. Then, the electron density is calculated from the single-electron wave functions and compared with the initial $n(\vec{r})_{trial}$. If these densities are converging, the ground-state of the system is found. If not, the $n(\vec{r})_{trial}$ must be updated. How this update looks and how to define $n(\vec{r})_{trial}$ together with explanation that tells how accurate the calculations need to be for the densities to converge, is set by different settings in the script that will run the program. This iterative method has also been developed through some years, and today, movement of ions is also allowed, resulting in so-called relaxed state calculations. In this project, both self-consistent field- and relaxed state calculations were performed (fig.2.2). For self-consistent field, the "old" version is applied, and only change of the electronic density takes place, while relaxed state calculations allow movement of the ions as well. Therefore, both the accuracy and computational time for self-consistent field calculations are reduced, compared to relaxed state calculations.

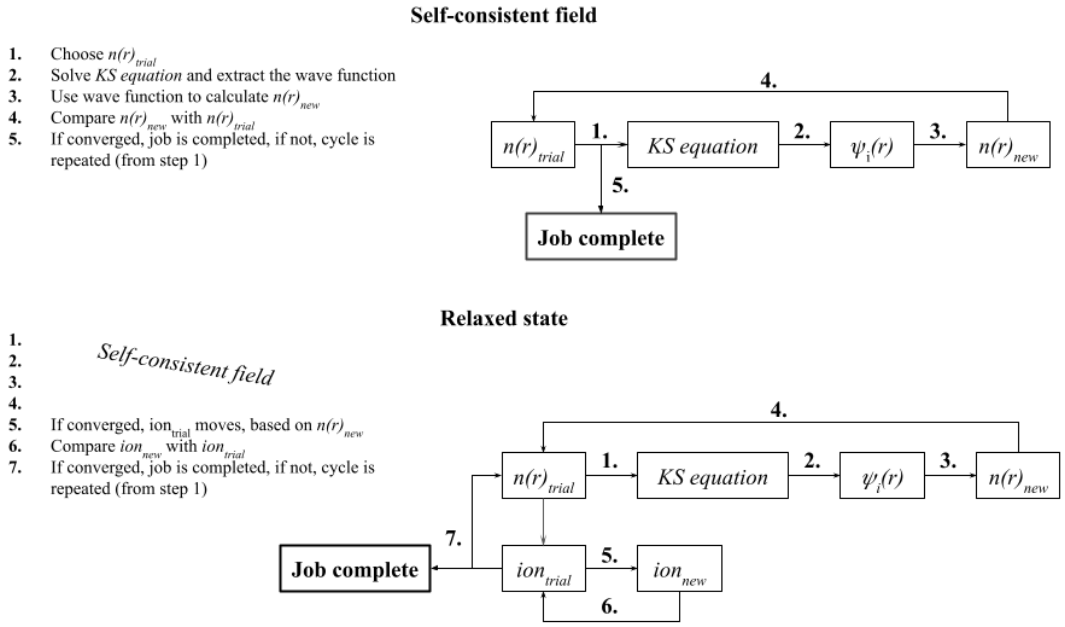

Figure 2.2: Schematic view of the steps in self-consistent field- and relaxed state calculations

2.3.1 Exchange-correlation functionals

In the KS equation the form of the exchange-correlation functional is unknown and is therefore treated in a approximate manner. A number of methods to define these functionals have been developed. The first approach was proposed by Kohn and Sham and is called the local density approximation (LDA) [36]. This assumes that the system consists of a uniform electron gas where the electron density is constant at all points in space

$$E_{xc}^{LDA}[n] = \int n(\vec{r})\epsilon_{xc}(n(\vec{r}))d^3r \tag{2.24}$$

with $\epsilon_{xc}(n(\vec{r}))$ as the exchange-correlation energy per particle in a homogeneous electron gas with density $n(\vec{r})$. This was further developed, by considering the spins of the electrons, into the local spin density approximation (LSDA) [38]

$$E_{xc}^{LSDA}[n_\uparrow, n_\downarrow] = \int n(\vec{r})\epsilon_{xc}(n_\uparrow, n_\downarrow)d^3r \tag{2.25}$$

Another approach is the generalized gradient approximation (GGA) [39]

$$E_{xc}^{GGA}[n_\uparrow, n_\downarrow] = \int n(\vec{r})\epsilon_{xc}(n_\uparrow, n_\downarrow, \nabla n_\uparrow, \nabla n_\downarrow)d^3r \tag{2.26}$$

This uses information from the LSDA together with a local gradient in the electron density. How this gradient is included in the equation could also vary and different GGA functionals therefore exist. Two of the most widely used is the Perdew-Wang functional (PW91) and the Perdew-Burke-Ernzerhof functional (PBE) [28]. Since this method accounts for the gradient of the density, it has become widely used for solid state calculations which often comprises of smaller distances such as covalent, ionic and metal bonds. However, with longer distances between particles, fluctuations of charges located far away from each other could cause van-der-Waals (vdW) interactions and these forces are not considered in GGA functionals [40]. The GGA approach is therefore a good method to describe solid-state system but becomes less accurate in soft matter structures, where many biological molecules are included. The Rutgers-Chalmers collaboration [41] has developed the so called van der Waals density functional (vdW-DF) which extends to nonlocal, long-ranged interactions without loosing information from the local and semi-local functionals. It involved a numbers of papers and 2004, the description of vdW-DF for general geometries was published [42]. The starting point was to divide the exchange-correlation energy into

$$E_{xc}[n] = E_x[n] + E_c[n] \tag{2.27}$$

where $E_x[n]$ is the contribution from the exchange term and $E_c[n]$ is the correlation energy. Both of these terms include nonlocal interactions, and the correlation term was further divided into

$$E_c[n] = E_c^0 + E_c^{nl} \tag{2.28}$$

where E_c^{nl} describes the long-range, nonlocal interactions and E_c^0 is approximated with LDA. E_c^{nl} was derived to

$$E_c^{nl} = \frac{1}{2} \int d^3r d^3r' n(\vec{r}) \phi(\vec{r}, \vec{r}') n(\vec{r}') \tag{2.29}$$

with $\phi(\vec{r}, \vec{r}')$ as a general (kernel) function depending on the distance between $|r - r'|$ and the densities n close to $\vec{r}$ and $\vec{r}'$. Expression and derivation of the kernel function is further described in Appendix I.

2.4 Theoretical summary and project constrains

Important highlights are the complexity of cells and the computational effort. One fundamental limitation of DFT is the association between number of atoms and time for calculation. Another challenge is an accurate description of the environment. Therefore, certain boundaries have been set in this project. All calculations have been performed at 0 K in vacuum without any interactions from the environment. The systems have also been set to perform relaxed- or self consistent field (SCF) calculations. Calculations for the relaxed state allow movements of both electrons and ions, until the optimal structure is found. SCF calculations keep the ions fixed, and only movement of electrons is allowed, which leads to less accurate outcome but a decrease in computational time. Therefore, to reach some results within a reasonable time frame, relaxation were performed to describe isolated system, id est, pairwise phospholipids and isolated G/GO layers. SCF calculations were performed with the purpose to analyze the isolated systems together, id est, interactions between phospholipid pairs and a G/GO layer.

3

Method of computation

My interest in performing density functional theory calculations for phospholipids in membranes was initiated by the practical experiments of Santosh et al.[11], which led to bacterial penetration from graphene flakes. The mechanisms behind these phenomena have not been further analysed and therefore, this work investigated the interactions with computational modeling. Calculations were carried out by Quantum ESPRESSO, an open source computer code implementation of DFT, plane waves and pseudopotentials [43][44][45][46]. The pseudopotantials (PP) for each atomic specie were picked from the GBRV packages and all the PPs were in unified PP format with the stored potentials as ultrasoft PP and the functional type as PBE [47]. The vdW-DF-cx [48][49][50][51] was used as the input functional for the exchange-correlation which overrides the values from the PP files. Their recommended cutoff kinetic energies for the wavefunctions and charge density where used with values of 40 respectively 200 Ry. All calculations were performed to the relaxed state, except for the system with double phospholipids and graphene/graphene oxide layers, which were set to perform self-consistence field (SCF) calculations. For the k-points, a 2-2-1 Monkhorst-Pack grid was used [52]. All calculations were set to $n_a \times 10^{-7} a.u$ for the electronic selfconsistency threshold, and for the relaxed state calculations, the convergence thresholds for the total energy and forces were set to $n_a \times 10^{-6} a.u$ (n_a = number of atoms).

The constituent and structure for each molecule was collected from the PubChem website [53]. The molecular structures were obtained in 2D and converted to 3D by relaxation. All calculations were carried out with periodically repeated unit cells. To isolate each system from interacting neighbours, a free Bravais-lattice with rectangular base (x,y) and orthogonal height (z) was used, so that all vectors intersected at 90°. The parameters for the unit cells were tailored to fit each system and the concerning molecules. The orthorhombic system is therefore considered and the length of each side will be referred as (x, y, z) Å in the description.

3.1 Graphene- and graphene oxide simulations

A graphene (G) and graphene oxide (GO) ”flake” were calculated in two separated systems. Both flakes were periodically repeated in the z-direction with the surface perpendicular to the y-direction, and ”cut” in the x-direction. The precise chemical structure of the edges of G/GO has been debated over the years and there is still no unambiguous model existing. This could be due to the lack of suitable analytical techniques for characterization, but also the fluctuation between different samples. The edges for the non-periodic sides were structured as a zigzag pattern with H atoms bonding to the edges [54]. The prediction of the distribution of functional groups on the GO layers was influenced by Anton Lerf and Jacek Klinowski, which published a model that has become the most well known today [55]. The constituents of the GO layer were obtained from the graphene supermarket [56]. The composition was specified to 79 weight% C and 20 weight% O. According to the Lerf-Klinowski model, most of the oxygen atoms are attached as epoxy-(-O-) and alcohol groups (-OH) [57]. It was therefore assumed that the rest (1 weight%) belonged to H atoms. The distribution of weight% was transferred into number of atoms/carbon. This was done by the following steps:

The Molar mass of each atom is

$$M_H = 1.008 \text{ g/mol}, \quad M_C = 12.011 \text{ g/mol}, \quad M_O = 15.999 \text{ g/mol} \tag{3.1}$$

and the equation for weight% can be written as

$$\frac{12.011 n_C}{m_T} = 0.79, \quad \frac{15.999 n_O}{m_T} = 0.20, \quad \frac{1.008 n_H}{m_T} = 0.01 \tag{3.2}$$

With n_i as the number of mols, M_i as the molar mass and m_T as the total mass. The formulas of Eq.3.2 were rearranged and the distribution of number of atoms were given as

$$\frac{n_O}{n_C} = 0.19, \quad \frac{n_H}{n_C} = 0.15 \tag{3.3}$$

The cell sizes for both flakes were set to (30.00, 8.00, 14.76) Å

3.2 Phospholipid simulations

3.2.1 Single phospholipids

A small library of four isolated phospholipids was created. They were hand-picked by their abundance in each organism. Phosphatidylglycerol (PG) and cardiolipin (CL) are two major constituents in bacteria membranes [19] while the outer leaflet of human membranes have high levels of phosphatidylcholine (PC) and sphingomyelin (SM) [17][18]. Calculations started by simulations of the "heads" from each phospholipid together with two carbons of each acyl chain (the "tail"). When the optimal state of each head-group was reached, the rest of the tails were introduced. The cell parameters were set to (40.00, 20.00 , 15.00) Å for isolated PC, PG, SM and (40.00, 40.00, 15.00) Å for CL.

3.2.2 Phospholipid pairs

The single phospholipids were simulated together with a second phospholipid from the same organism, for analysis of the interactive energy between different phospholipids. In plasma membranes, multiple phospholipids interact in a parallel manner, but the exact positions (rotations) between phospholipids is not defined. Therefore, we assume parallel stacking in the horizontal direction (from the tail to head), and all rotations of the horizontal axis of each phospholipid is allowed. In this project, the initial positions of the paired phospholipids, PC/PC, PC/SM, PG/PG and SM/SM, were obtained by introducing one single phospholipids into another single phospholipid, and then, one of the phospholipids was moved 10.00 Å in the y-direction. For CL/CL and CL/PG, CL was moved 10.00 Å in the z-direction. The cell parameters were set to (40.00, 25.00, 15.00) Å for PC/PC, PC/SM, SM/SM, PG/PG and (40.00, 25.00, 25.00) Å for CL/CL and PG/CL.

3.3 Simulations of graphene and phospholipid interactions

Analysis of the interaction between the phospholipid pairs to the G/GO flakes were also calculated. These simulations were performed with SCF calculations via a number of steps. First, calculations of approaching G/GO flakes to the head groups of the phospholipid pairs were performed. The zero distance of the G/GO layers in the x-direction, was set so that the edge of the G/GO layers was at the same position as the atom of largest x-value of the phospholipid pair. In y-direction, the G/GO layers were set between "the gap" of the interactive heads. Eight steps were calculated, from 7 Å down to 0 Å in the x-direction. Further, the two phospholipids in each system were separated in the y-direction, and the G/GO layers were simultaneously moved in both the y- and x-direction. This was done to allow the G/GO flakes to penetrate the phospholipid pairs. Therefore, both the separation distance between the phospholipids, and the penetration depth of the G/GO flakes were analyzed. Separation of the phospholipid pairs were done with added distances of 3, 4, 5, 6, 7 and 8 Å in the y-direction. The G/GO layers were simultaneously moved half of that distance in the y-direction. Penetration of the G/GO between the phospholipid pairs was performed by moving the G/GO flakes in the x-direction, with distances of 0, 2, 4, 6, 8, 10, 12 Å. The output was matrices of interaction energy for each system, with variables as added separation distance between the phospholipid pairs, and penetration depth of the G/GO flakes. The cell parameters were tailored for each system, so that the no interaction took place between repeated cells.

3.4 Calculation of bonds and interactions

The bonding between molecules were calculate by the formula

$$E_{bond} = E_{tot} - \sum_{i}^{N} E_i \tag{3.4}$$

with E_{tot} as the total energy for the whole system and E_i as the energy from the isolated molecules. The units for the energy in the output-file where given in Rydberg (Ry). The obtained value for $E_{bonding}$ where converged to electron volt (eV) and kilojoule per mol (kJ/mol).

3.5 Visualization

The open source code XCrySDen was used for visualization of the molecular structures. The software shows isosurfaces and contours of the atoms which can be interactively manipulated through rotation, colours, atomic radii and thickness of bonds [58].

4

Results and discussion

This chapter presents results from the SCF- and relaxed state calculations, and follows the work-flow of the project. The first section illustrates relaxation of each phospholipid in a single isolated form. These were used as the initial molecular structures for simulation of the phospholipid pairs to relaxation, and results from these calculations are presented in section 4.2. The last section (4.3) of this chapter included results from G/GO interactions with the paired phospholipids, which were all performed with SCF calculations.

4.1 Single Phospholipids

This section presents the outcome from the relaxed state calculations of each single phospholipids. Fig.4.1 illustrates the isolated phospholipids that were used as the initial molecular structure for the system of phospholipid pairs.

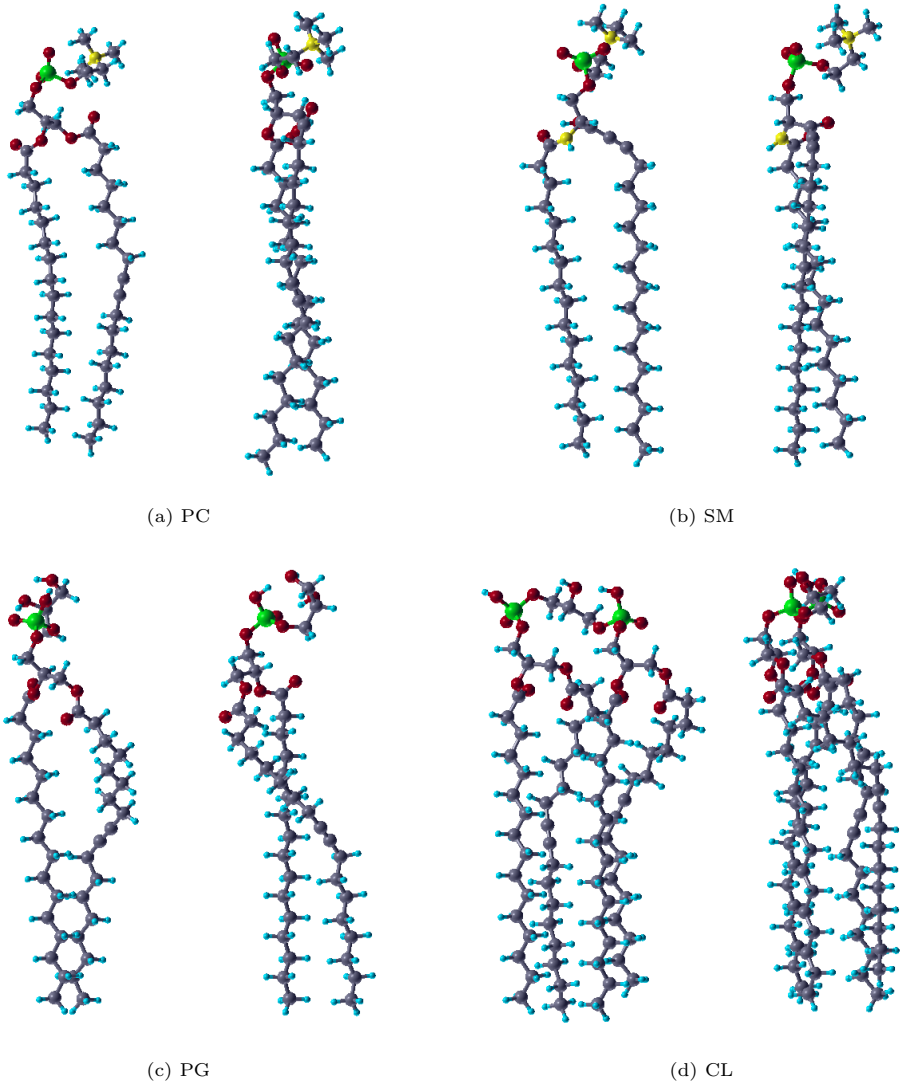

(a) PC

(b) SM

(c) PG

(d) CL

Figure 4.1: Visualization of the optimal structure of each phospholipid from two different angles

4.2 Phospholipid pairs

The single phospholipids were put together into systems of pairs, and further relaxed. PC/PC, PC/SM and SM/SM were simulated as the mammalian plasma membrane, while PG/PG, CL/CL and CL/PG were created as the bacterial membrane. However, the two systems, CL/CL and CL/PG did not managed to finish within the time-frame of this project, and are therefore not present in this section. The most reasonable explanation for this, is that, CL contains approximately twice as many atoms compared to all the other phospholipids, and thus, the time for relaxation will be increased.

Table 4.1: Interaction energy between paired phospholipids.

	Phospholipid pairs			
	Mammalian			**Bacteria**
Energy	PC/PC	PC/SM	SM/SM	PG/PG
kJ/mol	-127	-167	-197	-47
eV	-1.32	-1.73	-2.04	-0.49

Table.4.1 shows the obtained energies between the interacting phospholipids. Binding energies between phospholipids of mammalian cells are significantly higher than for bacterial phospholipids. The structure of each system is visualized in fig.4.2. Stacking of the bacterial pair seems to be straighter with a larger gap between them, while the mammalian pairs stacks closer to each other with tilting head-groups. For the PC/SM pair, an overlap in the hydrocarbon tails also takes place, which allows for a denser stacking.

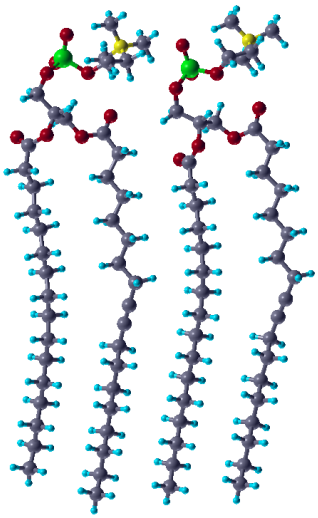

(a) PC/PC

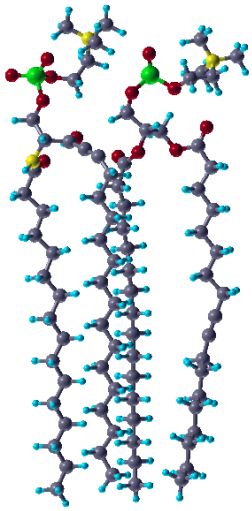

(b) PC/SM

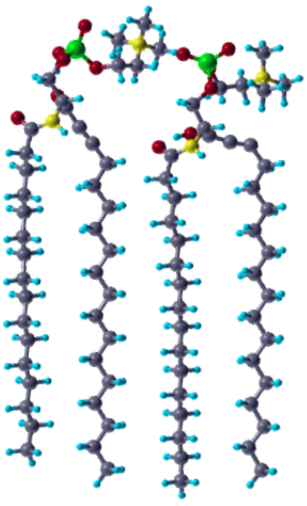

(c) SM/SM

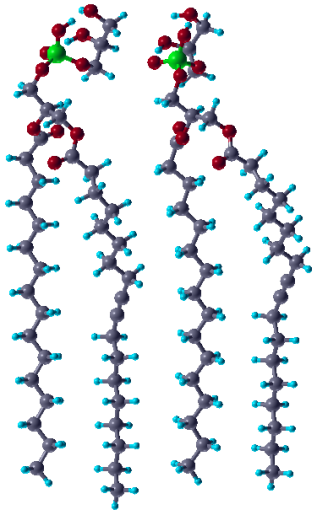

(d) PG/PG

Figure 4.2: Visualization of paired phospholipids

Further, investigation into the head-groups was carried out, to estimate their contribution to the interaction energy. Fig.4.3 shows some distances within the paired head-groups. The distances from PG/PG indicates a larger gap between the head groups, while the mammalian phospholipids have closer interactions with their neighbours phosphate group, and thus the tilting heads. An interesting finding was how the hydroxides (OH) in the PG/PG molecules arranged into H-bondings within its molecular structure (fig.4.3e). This could also explain why the distance between two PG molecules is more open and less robust. The head of PC/PC and PC/SM have more H-atoms and higher competition to available O-atoms of the same molecule, and thus tilting towards their neighbours for higher availability of interactions.

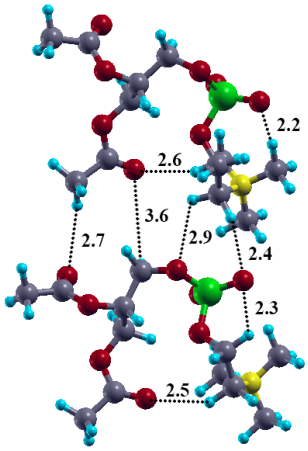

(a) Head of PC/PC

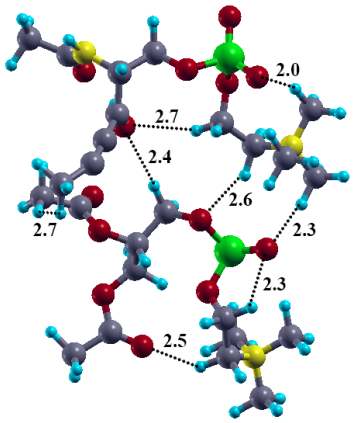

(b) Head of PC/SM

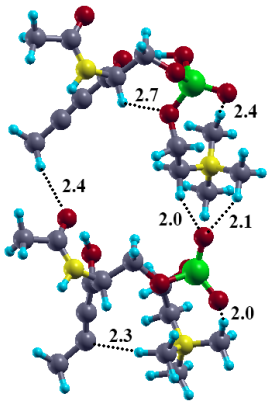

(c) Head of SM/SM

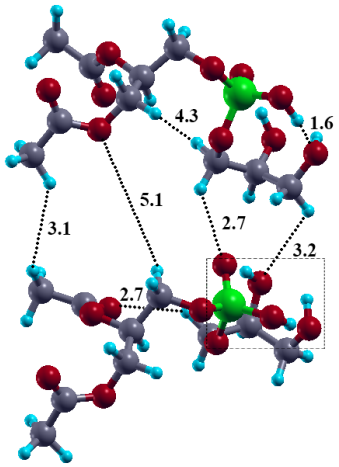

(d) Head of PG/PG

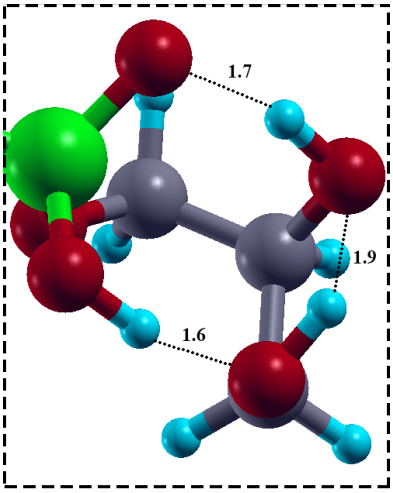

(e) Head of PG/PG with magnified view of the OH arrangement

Figure 4.3: The head groups of each phospholipid and some distances between close atoms, (a) PC/PC, (b) PC/SM, (c) SM/SM (d) PG/PG with (e) magnified image of the OH arrangement in PG/PG.

4.3 Graphene/graphene oxide interactions with paired phospholipids

We are interested in the interaction of the G/GO flakes with the phospholipid, both when the flakes approaches the membrane, and upon penetration. First, we study the approaching flakes by calculating the interaction energy between G/GO and a phospholipid pair, as illustrated in fig.4.4. For the phase when G/GO enters the the membrane, the two phospholipids are separated before calculating the interaction energy, fig.4.6.

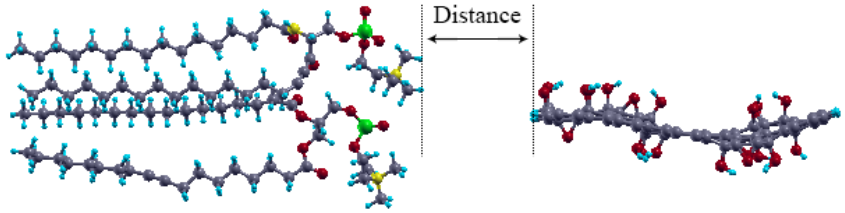

Figure 4.4: Visualization of the defined distance between the approaching G/GO flakes and the phospholipid pairs

In fig. 4.5, the interaction energies of the phase of G/GO approaching the heads of the phospholipid pairs are plotted. Negative values (y-axis) represent attractive forces between the head of the phospholipids and the G/GO layer. All systems seem to have the most stable (lowest energies) at a distance of around 1 Å, except for the PC/PC pair. The deviation of PC/PC from this trend could be explained by the choice of the zero distance value. When G/GO approaches the lipid pair, energies are increasing and positive values are found, which indicate repulsive forces. Since these systems are evaluated by SCF calculations, ions cannot move, and thus, the repulsive forces are expected. The major difference between the systems is that the diverse response between the pairs takes place at a longer distance when GO is approaching (broader gap in y-direction). GO has functional groups attached to the surface, which might interact with the head of the phospholipids further away, compared to the pure G layer.

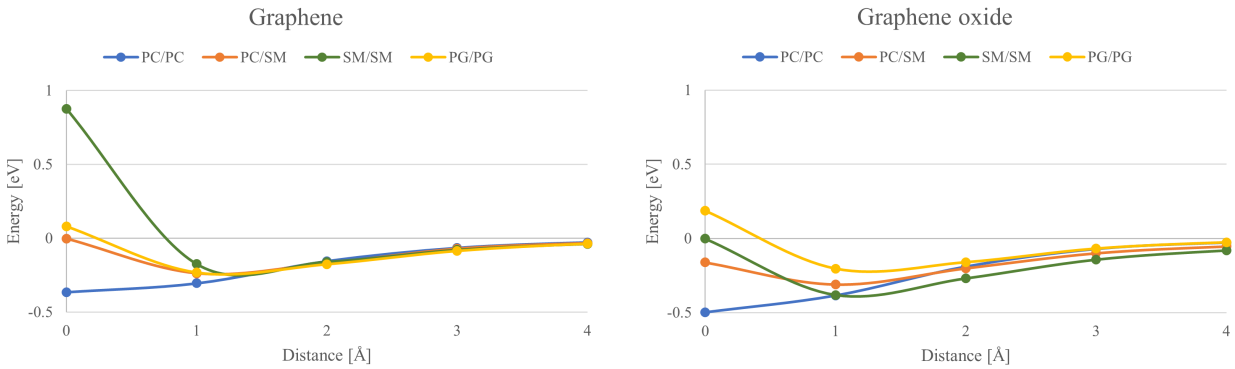

(a) G approaching paired phospholipids

(b) GO approaching paired phospholipids

Figure 4.5: Interaction energy when a) G and b) GO approach paired phospholipids.

Further, analysis of penetration depth was performed, in this case, simultaneously by separating the phospholipids with different distances (fig.4.6). This gave a matrix for each system, with the objective value as energy and variables as the penetration depth and added separation distance between the phospholipids.

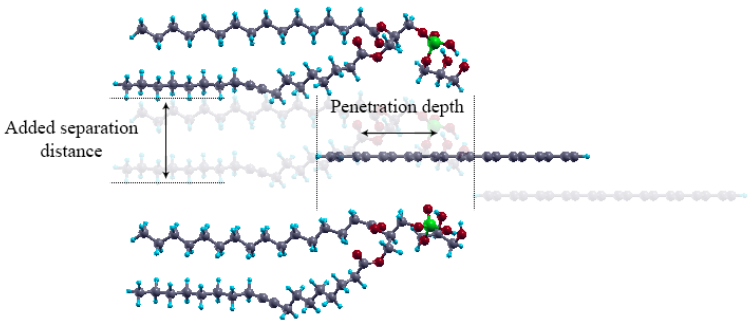

Figure 4.6: Visualization of how the phospholipids where separated simultaneously as penetration of the G/GO flakes.

Fig. 4.7 shows results from the phospholipid separation and G penetration. There are major contrasts between the bacterial pair (PG/PG) compared to all the mammalian pairs (PC/PC, PC/SM, SM/SM). The white colour represents high repulsive forces, and these are not visualized for the bacterial pair. The dark regions represent negative values, thus, attractive forces. These dark regions have more features in the bacterial systems, and indicate that the phospholipid pair needs less separation to be stable when G is penetrating. For the PC/SM and SM/SM, the energy never goes negative (E_{min} = 0.97 eV and E_{min} = 0.39 eV), and the insertion of G does not result in attractive forces. For the PC/PC pair the optimal choice of added separation distance, with the lowest energy, shows a small attraction ($E_{min} = -0.05$ eV), while the PG/PG pair exhibits an attraction one order of magnitude larger ($E_{min} = -0.54$ eV). The latter is thus a much more stable system. Fig.4.8 presents systems for GO penetration. Similar contrasts are found between the mammalian and bacterial pairs as in the G system. However, more of the situations calculated are repulsive, thus the white areas, where the largest difference between G and GO seems to be for the bacterial systems. When G was incorporated into the PG/PG pair, no white colour appeared in the figure, but for the system with GO, the PG/PG pair seems to experience repulsive forces just as for the mammalian pairs. However, the dark regions, with attractive energies, are still more prominent for the bacterial pair, compared to all the mammalian systems. The most stable for GO penetration is still the PG/PG pair ($E_{min} = -0.35$ eV). The lowest energies for PC/SM (E_{min} = 0.95 eV) and SM/SM (E_{min} = 0.48 eV) are still positive and the PC/PC pair experience small attractive forces ($E_{min} = -0.06$ eV).

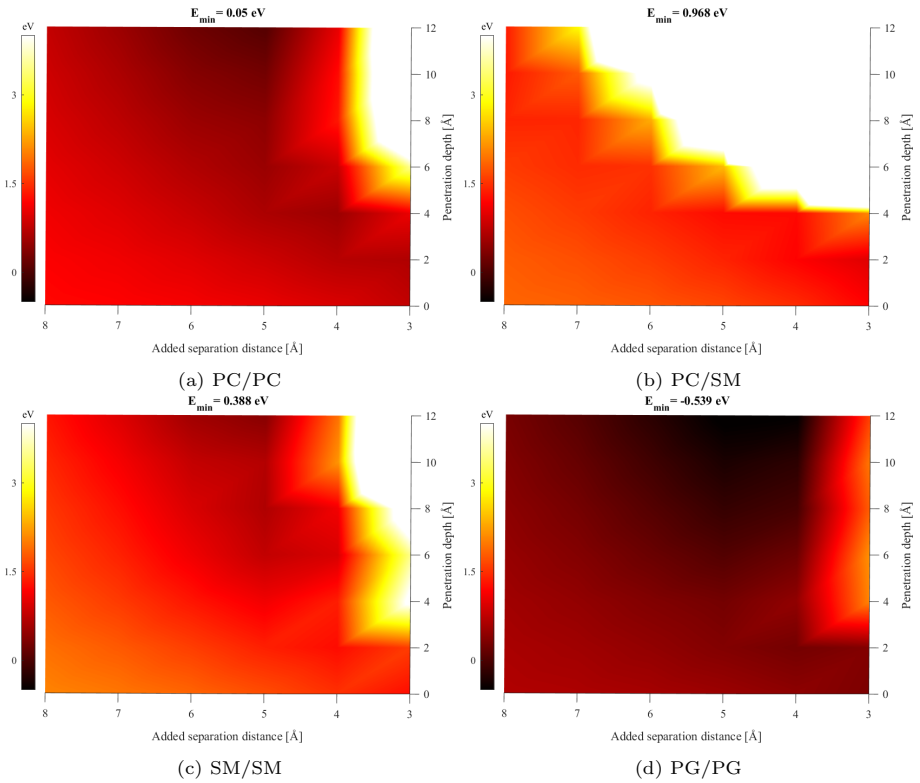

(a) PC/PC (b) PC/SM

(c) SM/SM (d) PG/PG

Figure 4.7: Interpolated interaction energies from the SCF calculations. The variables are the added separation distances between the phospholipid pairs and the penetration depths of the G layers.

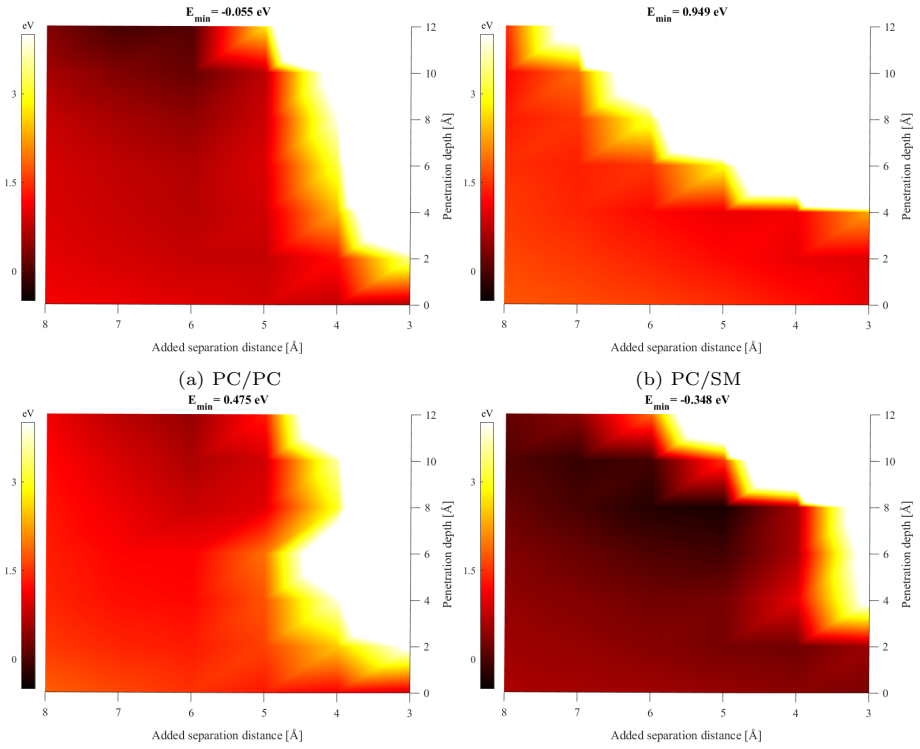

(a) PC/PC

(b) PC/SM

(c) SM/SM

(d) PG/PG

Figure 4.8: As for fig.4.7, but for GO intercalation

5

Conclusion and perspectives

5.1 Analysis of result

From these results, some conclusion can be taken. Interaction between the pairs seems to be highly effected by the constituents in the head-groups. All mammalian phospholipids have stronger interactions to another mammalian phospholipid compared to the bacterial phospholipid pair. However, it should be stated that only one system was completed for the bacterial pairs, and thus, we only have one system to compare against. It also seems that with more OH-groups in the head, a "special" arrangement takes place, which indicates on higher intramolecular attractions, and less intermolecular force between phospholipid pairs. This could be visualized by the distances between the head-groups (fig4.3). When the G and GO flakes approach the phospholipid pairs, nothing significant seems to happen between the systems. From the interpolated interaction energies (fig.4.7 and fig.4.8), it can be stated that the bacterial pair needs less separation to experience attractive forces to both G and GO penetration, compared to all the mammalian pairs. Therefore, weaker interactions between the phospholipid pair, and stronger attraction to G could be factors to the diverse robustness between bacterial and mammalian cells.

5.2 Outlook

Even if the calculations indicate a possible cause of viability between bacterial and mammalian cells to graphene, the environmental conditions are not included in the simulations. However, this is something that can be added for future simulations, and it would be of relevance to explore how much environmental conditions can effect the outcome of calculations. Another consideration, calculations in this project are done between two phospholipids, and in reality, phospholipids interact with multiple neighbours. Therefore, rotations between phospholipids and stacking of more phospholipids are suggestions for future investigations. In the SCF calculations, movement of ions are not allowed, and thus, performance with relaxed state calculations and/or molecular dynamics would be closer to reality.

Bibliography

[1] Francesco Pappalardo et al. "In silico clinical trials: concepts and early adoptions". In: *Briefings in Bioinformatics* 20.5 (June 2018), pp. 1699–1708. ISSN: 1477-4054. DOI: https://doi.org/10.1093/bib/bby043.

[2] Jens Nielsen and Jay D. Keasling. "Engineering Cellular Metabolism." In: *Cell* 164.6 (2016), pp. 1185–1197. DOI: https://doi.org/10.1016/j.cell.2016.02.004.

[3] M. Aldeghi and P.C. Biggin. "3.02 - Advances in Molecular Simulation". In: *Comprehensive Medicinal Chemistry III*. Ed. by Samuel Chackalamannil, David Rotella, and Simon E. Ward. Oxford: Elsevier, 2017, pp. 14–33. ISBN: 978-0-12-803201-5. DOI: https://doi.org/10.1016/B978-0-12-409547-2.12343-1.

[4] David J. Huggins et al. "Biomolecular simulations: From dynamics and mechanisms to computational assays of biological activity". In: *WIREs Computational Molecular Science* 9.3 (2019), e1393. DOI: https://doi.org/10.1002/wcms.1393.

[5] Kara Rogers and Robert J Kadner. *Bacteria*. 2020. URL: https://www.britannica.com/science/bacteria. (accessed: 25.01.2022).

[6] John M. Archibald. "Endosymbiosis and Eukaryotic Cell Evolution". In: *Current Biology* 25.19 (2015), R911–R921. ISSN: 0960-9822. DOI: https://doi.org/10.1016/j.cub.2015.07.055.

[7] Europe World Health Organization. *Communicable diseases*. URL: https://www.euro.who.int/en/health-topics/communicable-diseases. (accessed: 04.04.2022).

[8] World Health Organization. *Antimicrobial resistance*. 2021. URL: https://www.who.int/news-room/fact-sheets/detail/antimicrobial-resistance. (accessed: 25.01.2022).

[9] Jessica L. Fraser et al. "Healthcare-associated outbreaks of bacterial infections in Africa, 2009–2018: A review". In: *International Journal of Infectious Diseases* 103 (2021), pp. 469–477. ISSN: 1201-9712. DOI: https://doi.org/10.1016/j.ijid.2020.12.030.

[10] Graphene Flagship. *The Graphene Flagship*. 2013. URL: https://graphene-flagship.eu/collaboration/about-us/the-graphene-flagship/. (accessed: 28.01.2022).

[11] Santosh Pandit et al. "Vertically Aligned Graphene Coating is Bactericidal and Prevents the Formation of Bacterial Biofilms". In: *Advanced Materials Interfaces* 5.7 (2018), p. 1701331. DOI: https://doi.org/10.1002/admi.201701331.

[12] Evitria. *Mammalian cell culture – Types and application*. 2021. URL: https://www.evitria.com/journal/cho-cells/mammalian-cell-culture/. (accessed: 11.05.2022).

[13] William F. Martin, Sriram Garg, and Verena Zimorski. "Endosymbiotic theories for eukaryote origin". In: *Philosophical Transactions of the Royal Society B: Biological Sciences* 370.1678 (2015), p. 20140330. DOI: 10.1098/rstb.2014.0330.

[14] Trudy M. Wassenaar. *Bacteria: The Benign, the Bad, and the Beautiful*. John Wiley and Sons, 2012. URL: https://ebookcentral.proquest.com/lib/chalmers/detail.action?docID=818466.

[15] Phospholipid Research Center. *The unique and different types of phospholipids*. URL: https://www.phospholipid-research-center.com/phospholipid/types/. (accessed: 14.04.2022).

[16] Phospholipid Research Center. *The various phospolipid aggregates*. URL: https://www.phospholipid-research-center.com/phospholipid/aggregates/. (accessed: 14.04.2022).

[17] Shin-ya Morita, Tokuji Tsuji, and Tomohiro Terada. "Protocols for Enzymatic Fluorometric Assays to Quantify Phospholipid Classes". In: *International Journal of Molecular Sciences* 21.3 (2020). ISSN: 1422-0067. DOI: 10.3390/ijms21031032.

[18] Giulio Preta. "New Insights Into Targeting Membrane Lipids for Cancer Therapy". In: *Frontiers in Cell and Developmental Biology* 8 (2020). ISSN: 2296-634X. DOI: 10.3389/fcell.2020.571237.

[19] Christian Sohlenkamp and Otto Geiger. "Bacterial membrane lipids: diversity in structures and pathways". In: *FEMS Microbiology Reviews* 40.1 (Apr. 2015), pp. 133–159. ISSN: 0168-6445. DOI: 10.1093/femsre/fuv008.

[20] K. S. Novoselov et al. "Electric Field Effect in Atomically Thin Carbon Films". In: *Science* 306.5696 (2004), pp. 666–669. DOI: https://doi.org/10.1126/science.1102896.

[21] K. S. Novoselov et al. "Two-dimensional atomic crystals". In: *Proceedings of the National Academy of Sciences* 102.30 (2005), pp. 10451–10453. DOI: https://10.1073/pnas.0502848102.

[22] A. K. Geim and K. S. Novoselov. "The rise of graphene". In: *Nature materials* 6 (2007), pp. 183–191. DOI: https://doi.org/10.1038/nmat1849.

[23] Ke Cao et al. "Elastic straining of free-standing monolayer graphene". In: *Nature Communications* 11.284 (2020). DOI: https://doi.org/10.1038/s41467-019-14130-0.

[24] A. K. Geim. "Graphene: Status and Prospects". In: *Science* 324.5934 (2009), pp. 1530–1534. DOI: https://doi.org/10.1126/science.1158877.

[25] Ramesh Rudrapati. "Graphene: Fabrication Methods, Properties, and Applications in Modern Industries". In: *Graphene Production and Application*. Ed. by Sadia Ameen, M. Shaheer Akhtar, and Hyung-Shik Shin. Rijeka: IntechOpen, 2020. Chap. 2. DOI: 10.5772/intechopen.92258. URL: https://doi.org/10.5772/intechopen.92258.

[26] Liangchuan Li et al. "Research Progress of the Liquid-Phase Exfoliation and Stable Dispersion Mechanism and Method of Graphene". In: *Frontiers in Materials* 6 (2019). ISSN: 2296-8016. DOI: https://doi.org/10.3389/fmats.2019.00325.

[27] Wolfram Koch and Max C. Holthausen. *A chemist's guide to density functional theory*. Wiley-VCH, 2001. ISBN: 3527304223. URL: https://search.ebscohost.com/login.aspx?direct=true&db=cat07470a&AN=clc.ba9924b5.5005.4786.a2d7.630166a46a58&site=eds-live&scope=site&authtype=guest&custid=s3911979&groupid=main&profile=eds.

[28] David S. Sholl and Janice A. Steckel. *Density functional theory : a practical introduction*. Wiley, 2009. ISBN: 9780470373170. URL: https://search.ebscohost.com/login.aspx?direct=true&db=cat07470a&AN=clc.98516e9a.ab0b.4a0e.9956.4148ca64567e&site=eds-live&scope=site&authtype=guest&custid=s3911979&groupid=main&profile=eds.

[29] E. Schrödinger. "An Undulatory Theory of the Mechanics of Atoms and Molecules". In: *Phys. Rev.* 28 (6 Dec. 1926), pp. 1049–1070. DOI: 10.1103/PhysRev.28.1049. URL: https://link.aps.org/doi/10.1103/PhysRev.28.1049.

[30] M. Born and R. Oppenheimer. "Zur Quantentheorie der Molekeln". In: *Annalen der Physik* 389.20 (1927), pp. 457–484. DOI: https://doi.org/10.1002/andp.19273892002. eprint: https://onlinelibrary.wiley.com/doi/pdf/10.1002/andp.19273892002. URL: https://onlinelibrary.wiley.com/doi/abs/10.1002/andp.19273892002.

[31] V. Fock. "„Selfconsistent field" mit Austausch für Natrium". In: *Zeitschrift für Physik* 60 (1930), pp. 795–805. DOI: https://doi.org/10.1007/BF01330439.

[32] Douglas Rayner Hartree and W. Hartree. "Self-consistent field, with exchange, for beryllium". In: *Proceedings of the Royal Society of London. Series A - Mathematical and Physical Sciences* 150.869 (1935), pp. 9–33. DOI: 10.1098/rspa.1935.0085. URL: https://royalsocietypublishing.org/doi/abs/10.1098/rspa.1935.0085.

[33] J. C. Slater. "The Theory of Complex Spectra". In: *Phys. Rev.* 34 (10 Nov. 1929), pp. 1293–1322. DOI: 10.1103/PhysRev.34.1293. URL: https://link.aps.org/doi/10.1103/PhysRev.34.1293.

[34] L. H. Thomas. "The calculation of atomic fields". In: *Mathematical Proceedings of the Cambridge Philosophical Society* 23.5 (1927), pp. 542–548. DOI: 10.1017/S0305004100011683.

[35] P. Hohenberg and W. Kohn. "Inhomogeneous Electron Gas". In: *Phys. Rev.* 136 (3B Nov. 1964), B864–B871. DOI: 10.1103/PhysRev.136.B864. URL: https://link.aps.org/doi/10.1103/PhysRev.136.B864.

[36] W. Kohn and L. J. Sham. "Self-Consistent Equations Including Exchange and Correlation Effects". In: *Phys. Rev.* 140 (4A Nov. 1965), A1133–A1138. DOI: 10.1103/PhysRev.140.A1133. URL: https://link.aps.org/doi/10.1103/PhysRev.140.A1133.

[37] NobelPrize.org. *The Nobel Prize in Chemistry 1998*. URL: https://www.nobelprize.org/prizes/chemistry/1998/summary/. (accessed: 03.04.2022).

[38] O. Gunnarsson and B. I. Lundqvist. "Exchange and correlation in atoms, molecules, and solids by the spin-density-functional formalism". In: *Phys. Rev. B* 13 (10 May 1976), pp. 4274–4298. DOI: 10.1103/PhysRevB.13.4274. URL: https://link.aps.org/doi/10.1103/PhysRevB.13.4274.

[39] Kieron Burke, John P. Perdew, and Matthias Ernzerhof. "Why the generalized gradient approximation works and how to go beyond it". In: *International Journal of Quantum Chemistry* 61.2 (1997), pp. 287–293. DOI: https://doi.org/10.1002/(SICI)1097-461X(1997)61:2<287::AID-QUA11>3.0.CO;2-9.

[40] Elisa Londero. *Theory of van der Waals bonding : from bulk materials to biomolecules*. Technical report MC2: 238. Department of Microtechnology and Nanoscience (MC2), Chalmers University of Technology, 2012. ISBN: 9789173857864. URL: https://search.ebscohost.com/login.aspx?direct=true&db=cat07470a&AN=clc.72ddd125.e2a7.4fdb.b541.24b52c00b022&site=eds-live&scope=site&authtype=guest&custid=s3911979&groupid=main&profile=eds.

[41] *vdW-DF activities*. URL: http://fy.chalmers.se/~schroder/vdWDF/. (accessed: 03.04.2022).

[42] M. Dion et al. "Van der Waals Density Functional for General Geometries". In: *Phys. Rev. Lett.* 92 (24 June 2004), p. 246401. DOI: 10.1103/PhysRevLett.92.246401. URL: https://link.aps.org/doi/10.1103/PhysRevLett.92.246401.

[43] Quantum ESPRESSO. *manifesto*. May 2021. URL: https://www.quantum-espresso.org/manifesto/.

[44] Paolo Giannozzi et al. "QUANTUM ESPRESSO: a modular and open-source software project for quantum simulations of materials". In: *Journal of Physics: Condensed Matter* 21.39 (Sept. 2009), p. 395502. DOI: 10.1088/0953-8984/21/39/395502.

[45] P Giannozzi et al. "Advanced capabilities for materials modelling with Quantum ESPRESSO". In: *Journal of Physics: Condensed Matter* 29.46 (Oct. 2017), p. 465901. DOI: 10.1088/1361-648x/aa8f79.

[46] Paolo Giannozzi et al. "Quantum ESPRESSO toward the exascale". In: *The Journal of Chemical Physics* 152.15 (2020), p. 154105. DOI: 10.1063/5.0005082.

[47] Kevin F. Garrity et al. "Pseudopotentials for high-throughput DFT calculations". In: *Computational Materials Science* 81 (2014), pp. 446–452. ISSN: 0927-0256. DOI: https://doi.org/10.1016/j.commatsci.2013.08.053.

[48] T. Thonhauser et al. "Spin Signature of Nonlocal Correlation Binding in Metal-Organic Frameworks". In: *Phys. Rev. Lett.* 115 (13 Sept. 2015), p. 136402. DOI: 10.1103/PhysRevLett.115.136402.

[49] T. Thonhauser et al. "Van der Waals density functional: Self-consistent potential and the nature of the van der Waals bond". In: *Phys. Rev. B* 76 (12 Sept. 2007), p. 125112. DOI: 10.1103/PhysRevB.76.125112.

[50] Kristian Berland et al. "van der Waals forces in density functional theory: a review of the vdW-DF method". In: *Reports on Progress in Physics* 78.6 (May 2015), p. 066501. DOI: 10.1088/0034-4885/78/6/066501.

[51] D C Langreth et al. "A density functional for sparse matter". In: *Journal of Physics: Condensed Matter* 21.8 (Jan. 2009), p. 084203. DOI: 10.1088/0953-8984/21/8/084203.

[52] Hendrik J. Monkhorst and James D. Pack. "Special points for Brillouin-zone integrations". In: *Phys. Rev. B* 13 (12 June 1976), pp. 5188–5192. DOI: 10.1103/PhysRevB.13.5188.

[53] National Library of Medicine. *PubChem*. URL: https://pubchem.ncbi.nlm.nih.gov/. (accessed: 05.04.2022).

[54] Amedeo Bellunato et al. "Chemistry at the Edge of Graphene". In: *ChemPhysChem* 17.6 (2016), pp. 785–801. DOI: https://doi.org/10.1002/cphc.201500926.

[55] Daniel R. Dreyer et al. "The chemistry of graphene oxide". In: *Chem. Soc. Rev.* 39 (1 2010), pp. 228–240. DOI: 10.1039/B917103G.

[56] GRAPHENE SUPERMARKET. *Ultra Highly Concentrated Single-Layer Graphene Oxide*. URL: https://www.graphene-supermarket.com/products/copy-of-ultra-highly-concentrated-single-layer-graphene-oxide-60-ml?pr_prod_strat=collection_fallback&pr_rec_pid=6931503055057&pr_ref_pid=6931500826833&pr_seq=uniform.

[57] Heyong He et al. "Solid-State NMR Studies of the Structure of Graphite Oxide". In: *The Journal of Physical Chemistry* 100.51 (1996), pp. 19954–19958. DOI: 10.1021/jp961563t.

[58] Anton Kokalj. "Computer graphics and graphical user interfaces as tools in simulations of matter at the atomic scale". In: *Computational Materials Science* 28.2 (2003), pp. 155–168. ISSN: 0927-0256. DOI: https://doi.org/10.1016/S0927-0256(03)00104-6.

A

Appendix I

The kernel of van der Waals density functional

From Eq. 2.29, $\phi(\vec{r},\vec{r}')$ was expressed as a general (kernel) function depending on the distance between $|r-r'|$ and the densities n close to $\vec{r}$ and $\vec{r}'$. The kernel is further expressed as

$$\phi(\vec{r},\vec{r}') = \frac{2me^4}{\pi^2}\int_0^\infty a^2 da \int_0^\infty b^2 db W(a,b) T(\nu(a),\nu(b),\nu'(a),\nu'(b)) \tag{A1}$$

where

$$T(w,x,y,z) = \frac{1}{2}\left[\frac{1}{w+x}+\frac{1}{y+z}\right]\left[\frac{1}{(w+y)(x+z)}+\frac{1}{(w+z)(y+z)}\right] \tag{A2}$$

and

$$W(a,b) = 2\frac{(3-a^2)b\cos(b)\sin(a)+(3-b^2)a\cos(a)\sin(b)+(a^2+b^2-3)\sin(a)\sin(b)-3ab\cos(a)\cos(b)}{a^3b^3} \tag{A3}$$

ν and ν' are given as

$$\nu(y) = \frac{y^2}{2h\,(y/d)} \tag{A4}$$

$$\nu'(y) = \frac{y^2}{2h\,(/d')} \tag{A5}$$

where

$$d = |r-r'|q_0(\vec{r}) \tag{A6}$$

$$d' = |r-r'|q_0(\vec{r}') \tag{A7}$$

$$h(y) = 1-e^{\gamma y^2} \tag{A8}$$

and q_0 is given as

$$q_0(\vec{r}) = \frac{\epsilon_{xc}^0(\vec{r})}{\epsilon_x^{LDA}(\vec{r})}k_F(\vec{r}) \tag{A9}$$

where

$$\epsilon_x^{LDA} = \frac{-3e^2k_F}{4\pi} \tag{A10}$$

and

$$k_F = (3\pi^2 n)^{\frac{1}{3}} \tag{A11}$$

ϵ_{xc}^0 is approximated by using a gradient correction to LDA

$$\epsilon_{xc}^0 = \epsilon_{xc}^{LDA} - \epsilon_x^{LDA}\left[\frac{Z_{ab}}{9}\left(\frac{\nabla n}{2k_F n}\right)^2\right] \tag{A12}$$

where

$$Z_{ab} = -0.8491 \tag{A13}$$

is the contribution from the screened response which was obtained from a diagrammatic analysis. Thus, the kernel depends on $\vec{r}$ and $\vec{r}'$, which can tabulated through d and d'. The exchange term in eq.2.27 lacks a unique description in the vdW-DF method, and therefore, this is defined through some physical requirements which needs to be met. Different models to describe this term exist and in this paper is the vdW-DF-cx used where cx stands for consistent exchange.

DEPARTMENT OF MICROTECHNOLOGY AND NANOSCIENCE (MC2)
CHALMERS UNIVERSITY OF TECHNOLOGY
Gothenburg, Sweden 2022
www.chalmers.se

Department of Microtechnology and Nanoscience (MC2)
CHALMERS UNIVERSITY OF TECHNOLOGY
Gothenburg, Sweden, 2022